第 43 卷 第 7 期/2023 年 4 月/光学学报 研究论文

光学学报

基于时序控制的赝热光鬼成像系统

宗岩峰，郑淮斌*，吴鑫伟，李经纬，邱龙，韩聿源

西安交通大学电子科学与工程学院电子陶瓷与器件教育部重点实验室，国际电介质研究中心，陕西 西安 710049

摘要 设计开发了用于赝热光鬼成像的时序可控系统，该系统能对赝热光鬼成像系统硬件进行精准的同步控制，从而对散斑尺寸和采样次数等影响成像质量的因素进行定量分析，实现不同条件下的高质量成像。同时在鬼成像系统中结合差分鬼成像、归一化鬼成像和正负关联成像，针对正负关联算法重构图像提出了二次优化方案，进一步提升了赝热光鬼成像系统的成像质量。通过实验验证了系统的时序控制性能和算法的优化效果。

关键词 成像系统；鬼成像系统；同步控制；成像算法；成像质量

中图分类号 O436 **文献标志码** A **DOI**：10.3788/AOS221781

1 引 言

鬼成像(GI)即关联成像，是一种区别于传统光学成像的方式，通过巧妙设计光学传递函数，利用光场的二阶乃至高阶关联性质实现物-像的空间对应，从而重构出图像。鬼成像通过对分别携带光场空间分布信息的参考光路和物体光强信息的信号光路进行关联运算，从而重构出物体的图像信息。1995年史砚华小组[1-2]利用纠缠光子对实现了鬼成像实验，自此鬼成像吸引了研究者们的广泛关注，基于经典光源的鬼成像[3-6]、计算鬼成像[7-9]的实现，极大地推动了鬼成像的研究和发展。近年来，鬼成像技术以其抗散射能力强、无透镜成像、可离物成像等优势，得到了一定的应用推广。从照明来看，鬼成像技术不再局限于光学波段，X射线鬼成像[10-12]、太赫兹鬼成像[13]、微波鬼成像[14]等技术方案相继实现。从关联媒介来看，除了光子鬼成像，电子鬼成像[15]、原子鬼成像[16]、中子鬼成像[17-18]等也得到了论证。在应用场景上，3D鬼成像[19]、街角鬼成像[20]、运动目标鬼成像[21-23]、水下目标鬼成像[24-25]、抗湍流鬼成像[26-27]、远距离鬼成像[28]、显微镜鬼成像[29-30]、抗散射鬼成像[31-32]等也被报道。这些需求也带来许多应用基础问题，如复杂环境下信号精确检测、快速成像等亟待解决的问题，对鬼成像系统的硬件设计和控制以及算法都提出了更高的要求。本文基于赝热光鬼成像技术方案，设计并开发了时序可控的赝热光鬼成像系统，通过对成像系统的主要部件进行精确控制，定量地研究影响赝热光鬼成像质量的因素，并基于此成像系统对比分析了差分鬼成像(DGI)[33]、归一化鬼成像[34]，对正负关联成像算法[35]的重构图像进行了二次优化。该研究为有效、高质量地成像提供参考。

2 基本原理

赝热光鬼成像的光路示意图如图1所示。激光经准直后由透镜聚焦入射到旋转的毛玻璃上，产生的赝热光由分束器分为信号光路和参考光路。信号光照射在透射型物体，由桶探测器收集其光强涨落信息I_s。参考光携带物体表面的光场空间分布信息$I_r(x,y)$，该信息由电荷耦合器件(CCD)记录。对两路信号进行关联运算，即可重构物体图像：

$$g^{(2)}(x,y)=\frac{\langle I_s I_r(x,y)\rangle}{\langle I_s\rangle\langle I_r(x,y)\rangle},\tag{1}$$

式中：$\langle\cdot\rangle$表示取均值。为便于数据处理，这里对$g^{(2)}(x,y)$进行初步变换：

$$G(x,y)=\frac{\left(g^{(2)}-g^{(2)}_{\min}\right)}{g^{(2)}_{\max}-g^{(2)}_{\min}},\tag{2}$$

式中：$G(x,y)$为变换后的图像；$g^{(2)}_{\max}$和$g^{(2)}_{\min}$分别是$g^{(2)}(x,y)$的最大值和最小值，本文后续实验均对鬼成像的初步结果进行了式(2)的变换，对成像结果的二次处理使得图像对比度大于1/3。

为提高鬼成像质量，该系统在算法上采用了差分鬼成像和归一化鬼成像来优化重构图像，并对正负关联的成像算法进行了验证和后续改进。文献[34]给出

收稿日期：2022-09-30；**修回日期**：2022-10-21；**录用日期**：2022-10-31；**网络首发日期**：2022-11-04

基金项目：陕西省创新团队项目(2018TD-024)、陕西省重点研发计划重点产业创新链(群)-工业领域(2019ZDLGY09-10)、中央高校基本科研业务费专项资金资助(xzd022020008)

通信作者：*huaibinzheng@xjtu.edu.cn

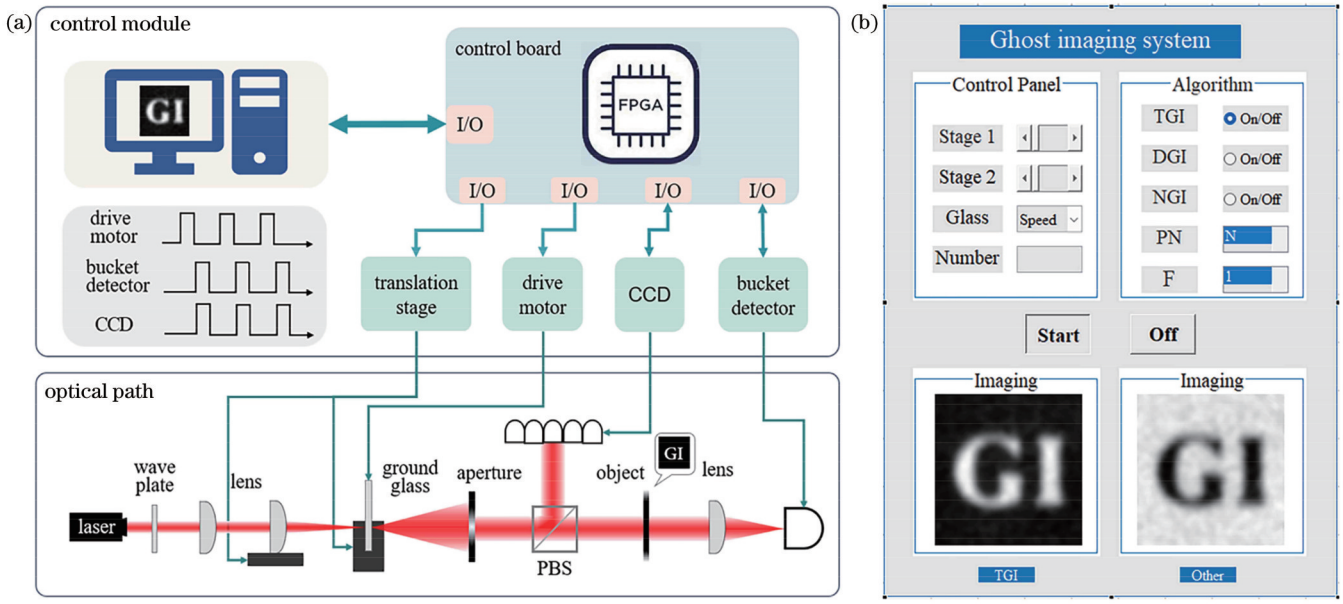

图 1　赝热光鬼成像系统。(a)系统示意图;(b) GUI界面

Fig. 1　Pseudo-thermal optical ghost imaging system. (a) System diagram; (b) GUI panel

了差分鬼成像和归一化鬼成像的重构算法,对于差分鬼成像,每一次迭代的结果为

$$O_i(x,y)=\left(I_s-\frac{\langle I_s\rangle}{\langle R\rangle}R\right)\left[I_r(x,y)-\langle I_r(x,y)\rangle\right],\tag{3}$$

式中:R为光场$I_r(x,y)$的光强。同样地,归一化鬼成像每一次的迭代结果为

$$O_i(x,y)=\left(\frac{I_s}{R}-\frac{\langle I_s\rangle}{\langle R\rangle}\right)\left[I_r(x,y)-\langle I_r(x,y)\rangle\right]。\tag{4}$$

最终的重构图像为所有迭代计算的平均,即$O(x,y)=\langle O_i(x,y)\rangle$。

根据文献[35]中的正负关联算法,以桶探测值的均值$\langle I_s\rangle$为判别条件,即

$$I_s=\begin{cases}I_{s+}, & I_s>\langle I_s\rangle\\ I_{s-}, & I_s<\langle I_s\rangle\end{cases}。\tag{5}$$

将光强值I_s和对应的$I_r(x,y)$分为两组并分别进行关联计算,由此可以重构出物体的正像$g_P(x,y)$和负像$g_N(x,y)$:

$$g_P(x,y)=\frac{\langle I_{s+}I_{r+}(x,y)\rangle}{\langle I_{s+}\rangle\langle I_{r+}(x,y)\rangle},\tag{6}$$

$$g_N(x,y)=\frac{\langle I_{s-}I_{r-}(x,y)\rangle}{\langle I_{s-}\rangle\langle I_{r-}(x,y)\rangle},\tag{7}$$

式中:$I_{r+}(x,y)$为I_{s+}对应的散斑;$I_{r-}(x,y)$为I_{s-}对应的散斑。对$g_P(x,y)$和$g_N(x,y)$进行类似式(2)的变换,得到正像$G_P(x,y)$和负像$G_N(x,y)$,对正像和负像作差,得到

$$G_{P\text{-}N}(x,y)=G_P(x,y)-G_N(x,y)。\tag{8}$$

对上述重构图像的算法进一步进行优化,进行类似式(2)的变换:

$$G(x,y)=\frac{G_{P\text{-}N}(x,y)-G_{noise}}{G_{max}-G_{min}}F,\tag{9}$$

式中:G_{noise}是噪声项;G_{max}和G_{min}是重构图像的灰度最大值和最小值;F是重构图像的灰度调控因子,通过改变F值调整降噪后的图像细节显示效果。

3　实　　验

3.1　实验装置与成像质量的表征

根据鬼成像原理,设计了如图1所示的赝热光鬼成像系统。图1(a)是赝热光鬼成像系统示意图;图1(b)是该系统的GUI界面,通过界面可直接控制系统的运行,如控制位移平台的位置、毛玻璃的转速、采样数量以及成像算法。赝热光鬼成像光路示意图中,将用作聚焦的平凸镜固定在可以纵向平移的电动位移平台上,位移平台可以实现高精度的距离控制和延时控制,这里通过控制位移平台调整平凸镜到毛玻璃的距离,改变照射在毛玻璃上的光斑大小,从而改变散斑的尺寸。毛玻璃由步进电机驱动旋转,转动速度可以由控制脉冲的频率决定,旋转周期根据步进电机可以设置为6400、3200、1600、800、400、200个脉冲时间,且毛玻璃置于横向的电动位移平台上,避免毛玻璃旋转的周期性造成探测光强的周期性变化,控制位移平台可以根据需求进行更多的有效采样。半波片和偏振分束器的组合使用,可以达到调节信号光和参考光功率的作用。将半波片光轴调至合适角度,使信号光功率达到最高,从而增大光强涨落幅度,提高鬼成像质量[36]。系统的同步控制和电动位移平台的控制由控制卡实现,同时完成信号的采集。系统的软件方面结合了差

分鬼成像、归一化鬼成像、正负关联算法及其优化算法，使鬼成像系统的性能得到进一步提升。

为了定量评价赝热光鬼成像的质量，本文使用了峰值信噪比（PSNR）、结构相似性（SSIM）、可见度、衬噪比（CNR）、直方图等多个指标来进行表征分析。图像的PSNR用来衡量图像失真水平或噪声水平，PSNR越大则图像失真越少。用E_{MS}表示均方差，PSNR定义为

$$R_{\mathrm{PSN}}=10\lg\left(255^2/E_{\mathrm{MS}}\right)。\tag{10}$$

结构相似性描述两幅图像之间的相似度，相似度越大表示鬼成像图像和待成像物体图像的差距越小，给定两幅图像x和y，SSIM定义[37]如下：

$$S_{\mathrm{SIM}}=\left[l\left(x,y\right)\right]^{\alpha}\left[c\left(x,y\right)\right]^{\beta}\left[s\left(x,y\right)\right]^{\gamma},\tag{11}$$

式中：$\alpha>0$，$\beta>0$，$\gamma>0$；$l\left(x,y\right)=2\mu_x\mu_y+c_1/\mu_x^2+\mu_y^2+c_1$是亮度，$c\left(x,y\right)=2\sigma_x\sigma_y+c_2/\sigma_x^2+\sigma_y^2+c_2$是对比度，$s\left(x,y\right)=\sigma_{xy}+c_3/\sigma_x+\sigma_y+c_3$是结构相似度，$\mu_x$、$\mu_y$和$\sigma_x^2$、$\sigma_y^2$分别是$x$和$y$的平均值和方差，$\sigma_{xy}$是$x$和$y$的协方差，$c_1$、$c_2$、$c_3$为常数。在此，设定$\alpha=\beta=\gamma=1$，$c_3=c_2/2$，得到简化的SSIM：

$$S_{\mathrm{SIM}}=\frac{\left(2\mu_x\mu_y+c_1\right)\left(2\sigma_{xy}+c_2\right)}{\left(\mu_x^2+\mu_y^2+c_1\right)\left(\sigma_x^2+\sigma_y^2+c_2\right)}。\tag{12}$$

可见度用来衡量图像的清晰程度，鬼成像图像的可见度越高，则视觉效果越好、越清晰，可见度的最大值为1，其定义式[38]为

$$V=\frac{\langle G_{\mathrm{s}}\rangle-\langle G_{\mathrm{b}}\rangle}{\langle G_{\mathrm{s}}\rangle+\langle G_{\mathrm{b}}\rangle},\tag{13}$$

式中：$\langle G_{\mathrm{s}}\rangle$和$\langle G_{\mathrm{b}}\rangle$分别为信号区和背景区的二阶相关函数的平均值。

衬噪比是对图像中信号区域和噪声背景区域之间对比度的衡量，其定义[39]为

$$R_{\mathrm{CN}}=\frac{\langle G_{\mathrm{s}}\rangle-\langle G_{\mathrm{b}}\rangle}{\sqrt{\sigma_{\mathrm{s}}^2+\sigma_{\mathrm{b}}^2}},\tag{14}$$

式中：σ_{s}^2和σ_{b}^2分别为信号区和背景区的二阶相关函数的方差。

3.2　实验结果与讨论

3.2.1　赝热光鬼成像系统的时序控制性能验证

根据上述所示的装置示意图，研制了时序可控的赝热光鬼成像系统。为了验证系统的时序控制性能，进行了散斑尺寸和采样数量对赝热光鬼成像质量影响的实验研究。

1）系统对散斑尺寸的控制及成像优化

研究表明，物体表面的散斑尺寸直接影响成像的质量[40-41]，而本系统可以精确控制纵向位移平台的移动，通过改变透镜到毛玻璃的距离，实现对散斑大小的精细调整，并对不同尺寸的物体实现最佳的成像质量。对不同尺寸的散斑进行20组实验，每组采样6400次，由CCD采样结果计算得到散斑尺寸。不同尺寸的散斑图及对应尺寸所重构的鬼成像如图2所示，字母“GI”的实际尺寸范围为0.20～0.80 mm，汉字“交”的实际尺寸为1.00 mm。

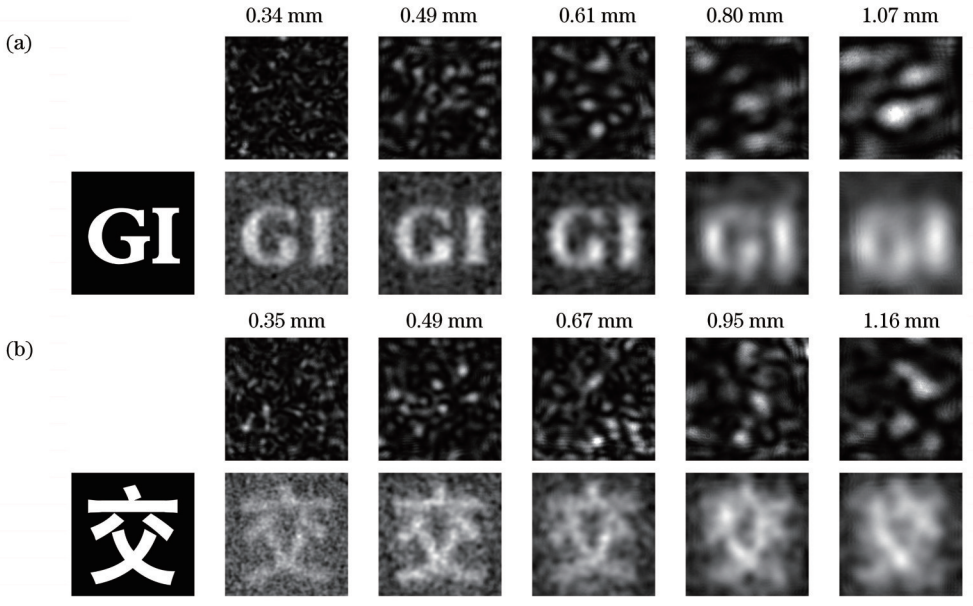

图2　不同散斑尺寸的赝热光鬼成像。(a)字母“GI”；(b)汉字“交”

Fig. 2　Results of pseudothermal ghost imaging for different size of speckle. (a) English letters "GI"; (b) Chinese character "jiao"

从图2可以看出，随着散斑尺寸的变化，赝热光鬼成像的质量有着明显的变化。用具体参数来客观地比较分析重构图像的质量变化，如图3所示。可以发现，对于不同尺寸的“GI”和“交”，其质量曲线有着不同的

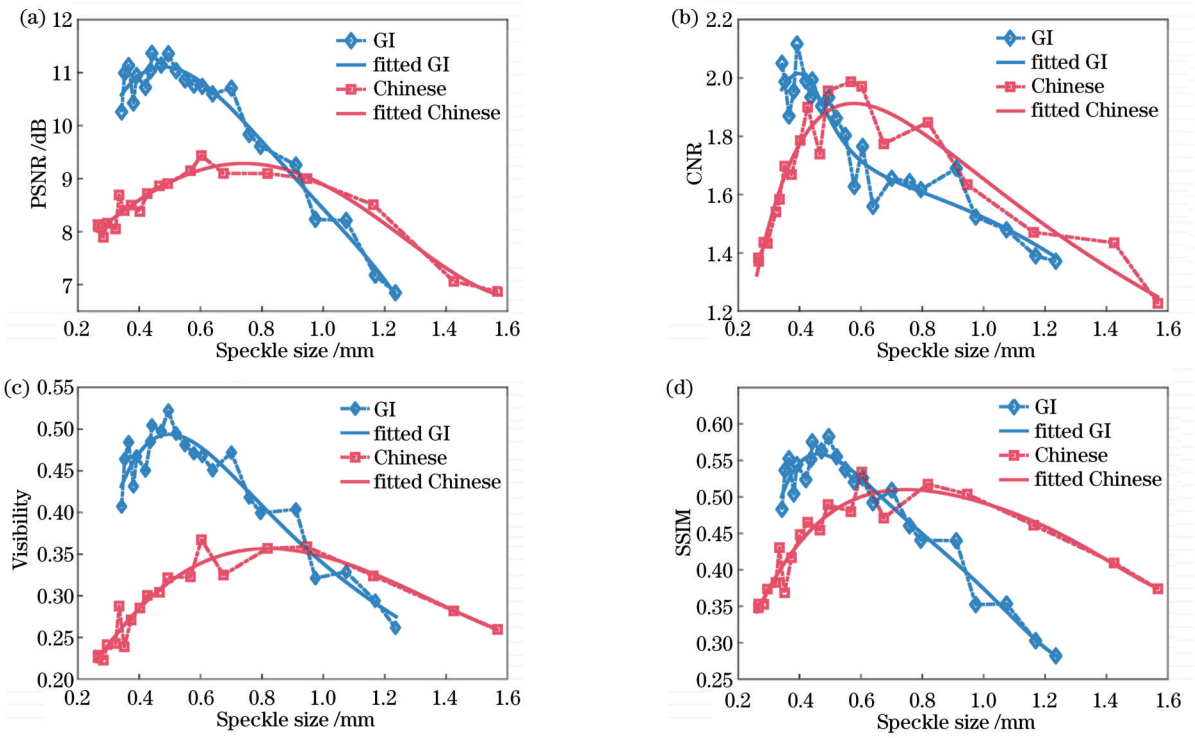

图 3　不同散斑大小下的鬼成像质量对比。(a) PSNR;(b) CNR;(c)可见度;(d) SSIM

Fig. 3　Comparison of ghost imaging quality for different size of speckle. (a) PSNR; (b) CNR; (c) visibility; (d) SSIM

极大值,二者对应的散斑尺寸也不尽相同,结果表明对于不同尺寸的物体,该系统可以通过调整散斑尺寸实现高质量的成像。

2)系统对采样数量的控制及成像优化

传统的赝热光鬼成像要通过足够多的采样才能实现较高质量的成像,本系统通过控制横向位移平台改变毛玻璃的位置,从而避免毛玻璃旋转造成采样数据的周期性,实现大量的有效采样,以此来提高成像质量。毛玻璃旋转周期设置为 3200 个脉冲时间,在 GUI 界面设置采样次数,对参考路和信号路同步进行数据采集,进行成像比较。图 4 是采样次数分别为 3200、10000、20000、50000、100000 时的赝热光鬼成像结果。

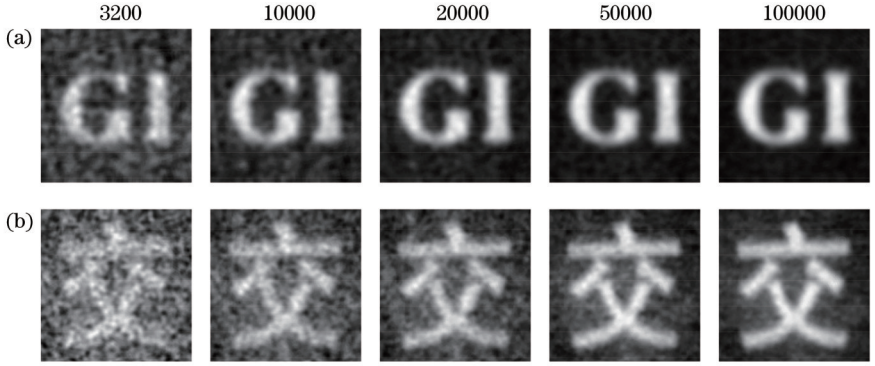

图 4　不同采样次数的赝热光鬼成像结果。(a)“GI”的不同采样次数下的重构图像;(b)“交”的不同采样次数下的重构图像

Fig. 4　Results of pseudo-thermal ghost imaging for different sampling times. (a) Images of "GI" for different sampling times; (b) images of "jiao" for different sampling times

重构图像的质量对比如图 5 所示。显而易见,当仅对毛玻璃旋转一周并进行采样后所重构的像并没有达到系统的最优成像质量,而当采样次数低于 20000 时,随着采样次数的增加,成像的质量始终在提高,图像的噪声更低,对比度更高,结构相似性也更好;只有当采样次数大于 20000 时,随着采样次数的增加,质量曲线变得平缓,成像质量基本不再有明显的提升,这是由赝热光的物理性质决定的[42]。通过实验成功证明了该系统的时序控制性能对传统赝热光鬼成像恢复更高质量图像的有效性。

3.2.2　赝热光鬼成像系统的算法验证

通过对系统的时序控制,可以调整最佳成像质量

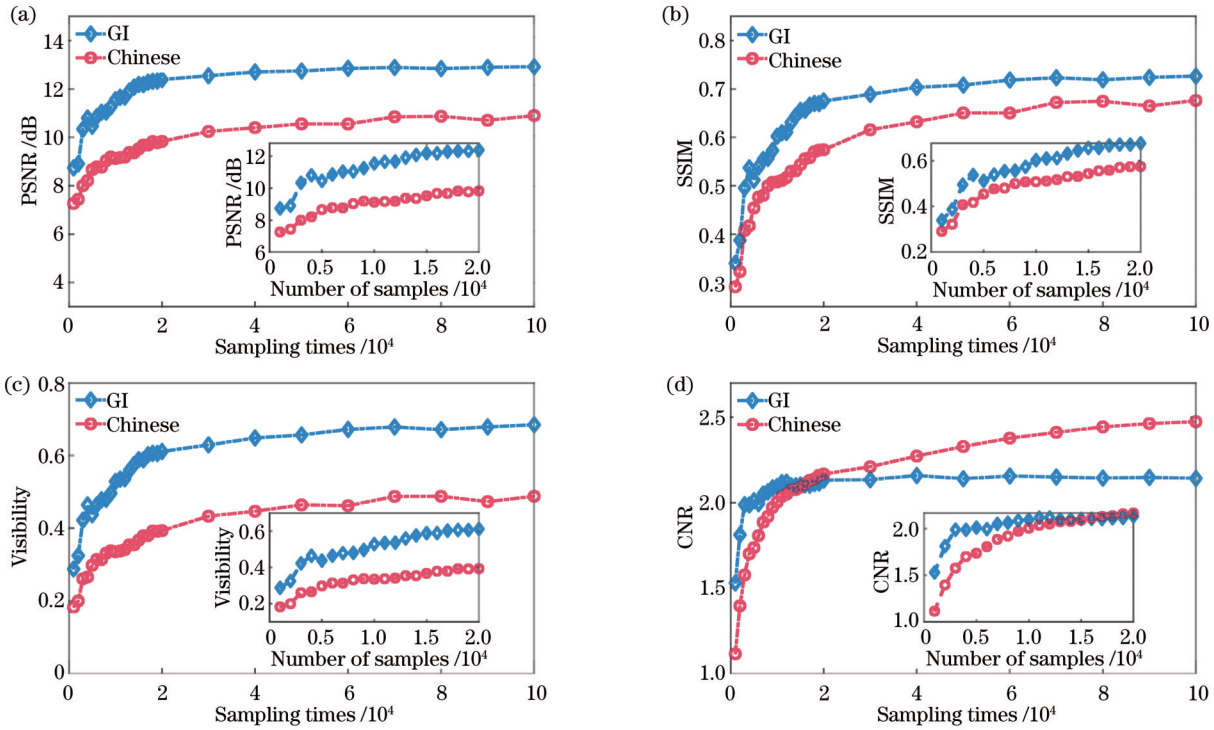

图 5　不同采样数量下的鬼成像质量对比。(a) PSNR;(b) SSIM;(c)可见度;(d) CNR

Fig. 5　Comparison of ghost imaging quality for different sampling times. (a) PSNR; (b) SSIM; (c) visibility; (d) CNR

的硬件设置。此外,该系统结合了不同算法,进一步提高传统赝热光鬼成像的成像质量。在 GUI 界面选择相应的成像算法,通过实验验证了差分鬼成像、归一化鬼成像、正负关联鬼成像对传统鬼成像(TGI)的质量优化。

1)差分鬼成像和归一化鬼成像

差分鬼成像、归一化鬼成像与传统鬼成像的成像质量结果对比如图 6 所示。观察可见,差分鬼成像和归一化鬼成像对于成像质量的优化效果近似,在图像上无明显差别。对于字母“GI”:当采样次数较少时,差分鬼成像和归一化鬼成像对于鬼成像质量略有改善,一定程度上达到了算法抑制背景噪声的目的;当采样次数较多时,大量的样本对于背景噪声有了一定的匀化,算法对于重构图像的质量优化效果则相对较差。而对于汉字“交”,差分鬼成像和归一化鬼成像的降噪效果则较为明显。

分别计算差分鬼成像和归一化鬼成像两种成像算法的 PSNR 和 SSIM,并与传统鬼成像进行对比分析,结果如图 7 所示。可以看出,差分鬼成像和归一化鬼成像的 PSNR 曲线和 SSIM 曲线基本重合,归一化鬼成像在降噪方面达到了类似差分鬼成像的效果,归一化鬼成像结果与文献[35]中的结论相符,即在大量采样的情况下,可将式(3)、(4)中$\langle I_s\rangle/\langle R\rangle$近似等于$\langle I_s/R\rangle$,从而有$\left\langle O_{\mathrm{NGI}}(x,y)\right\rangle=\left\langle O_{\mathrm{DGI}}(x,y)\right\rangle/\langle R\rangle$,其中$O_{\mathrm{NGI}}(x,y)$、$O_{\mathrm{DGI}}(x,y)$分别为 NGI 图像和 DGI 图像。对于不同类型的物体,差分鬼成像提高成像质量的效果也不一样,对于强透射型的物体,差分鬼成像的降噪效果更佳。

2)正负关联鬼成像

正负关联鬼成像同样具有一定的降噪效果,利用该系统进行正负关联鬼成像实验,得到正像(G_P)、负像(G_N)和二者的差像($G_{P\text{-}N}$),其与传统鬼成像的结果对比如图 8 所示。

在正负关联的基础上,对重构图像进行进一步的降噪处理。对重构图像进行式(7)所示的优化,可以发现赝热光鬼成像的噪声得到显著降低,信噪比提升较大,通过调整式(7)中的调控因子 F 调整成像质量,如图 9 所示。

观察图 9 可以看到上述实验对正负关联成像有显著的降噪效果,通过改变调控因子的值,可避免降噪过程中物体的部分信息丢失严重,图 10 用图像直方图对以上的结果进行比较说明。其中正负关联成像在采样数较少时的直方条分布没有明显区分,背景噪声分布范围较大,此时的成像中目标信息淹没在噪声中,图像模糊;成像质量得到提高后,图像的灰度值分布出现明显的两极分化,基本集中在灰度最大和最小值部分,因此图像中的物体信息更加清晰。对比变换后的正负关联成像发现,背景噪声减小了,图像信噪比得到极大的提高。

实验结果表明,在系统的时序控制可提升传统赝热光鬼成像质量的基础上,结合不同的算法,成像质量可得到进一步的提升。

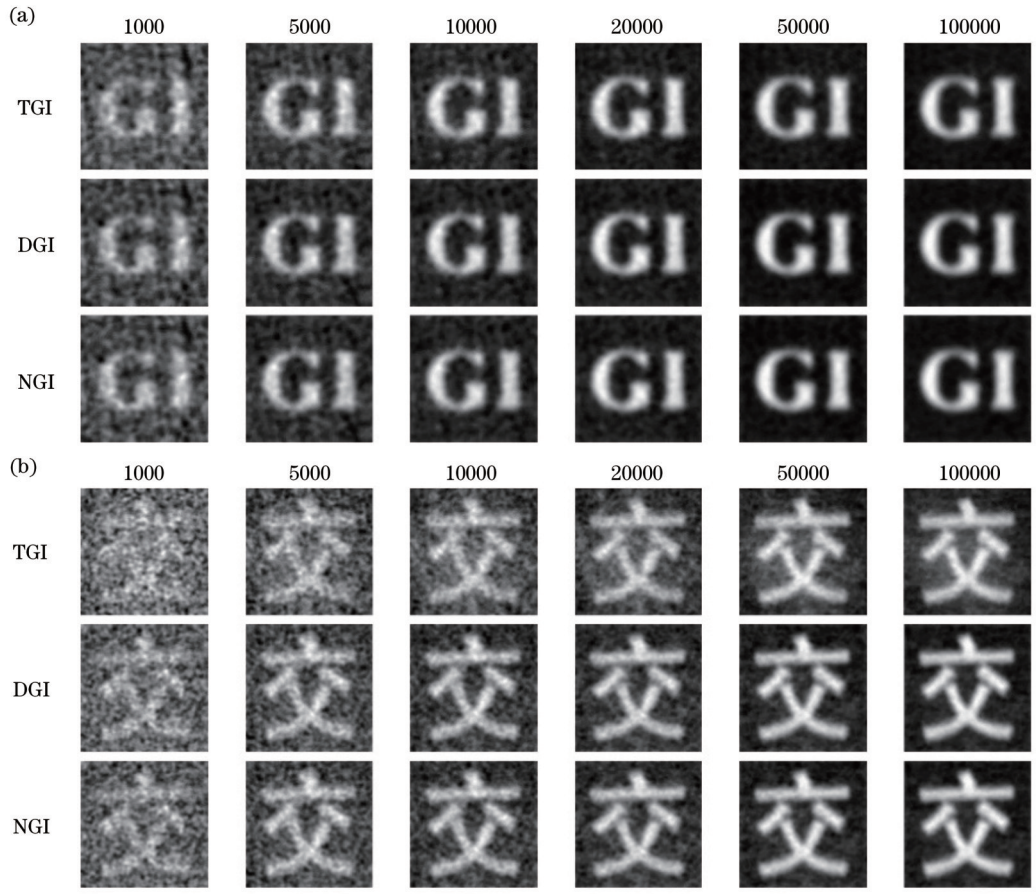

图 6　两种物体在不同采样次数下的 TGI、DGI 和 NGI 对比图。(a)字母“GI”;(b)汉字“交”

Fig. 6　Comparison of TGI, DGI, and NGI for two objects with different sampling times. (a) English letters "GI"; (b) Chinese character "jiao"

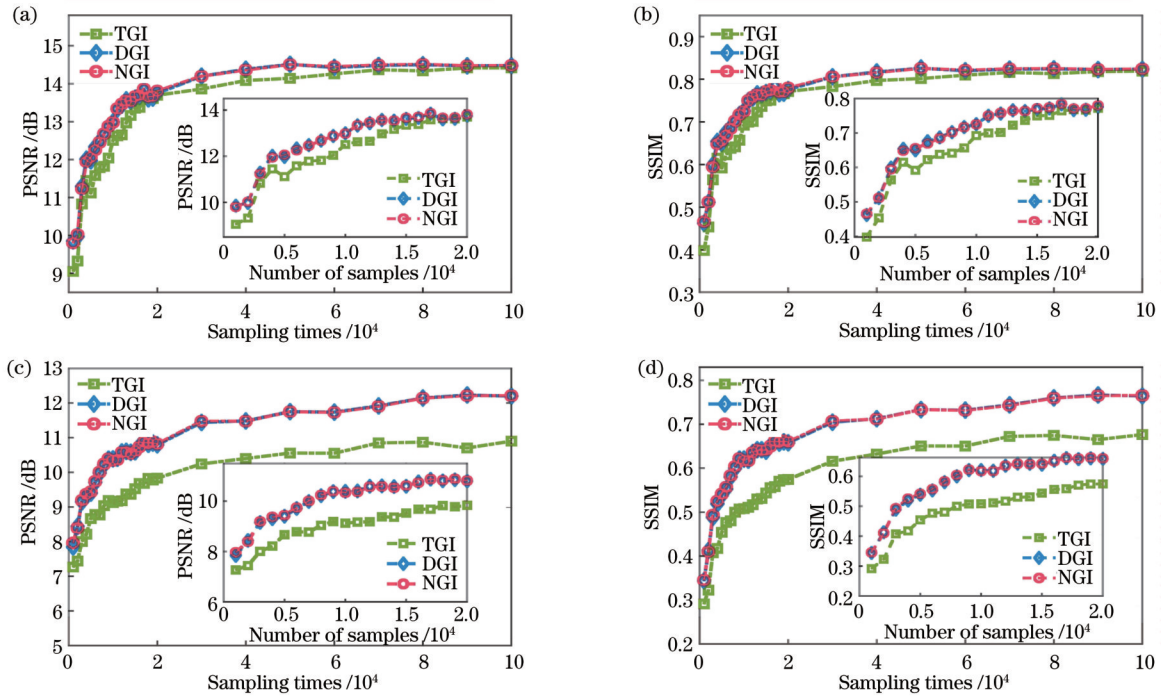

图 7　两种物体在不同采样次数下的 TGI、DGI 和 NGI 的成像质量对比。(a)(b) “GI”的 PSNR 和 SSIM 对比;(c)(d)“交”的 PSNR 和 SSIM 对比

Fig. 7　Imaging quality comparison of TGI, DGI, and NGI for two objects with different sampling times. (a)(b) Comparison of PSNR and SSIM for "GI"; (c)(d) comparison of PSNR and SSIM for "jiao"

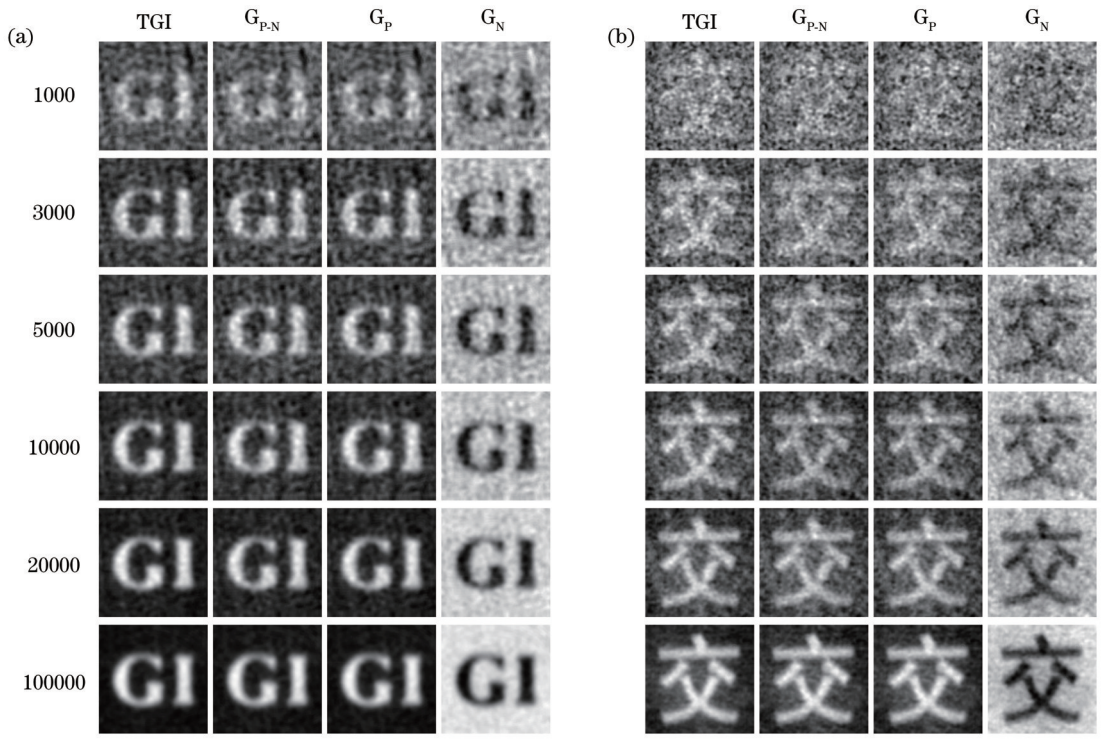

图 8　传统鬼成像和正负关联成像结果对比。(a)“GI”的成像对比;(b)“交”的成像对比

Fig. 8　Comparison of TGI and positive-negative correlation imaging results. (a) Comparison of imaging results of "GI"; (b) comparison of imaging results of "jiao"

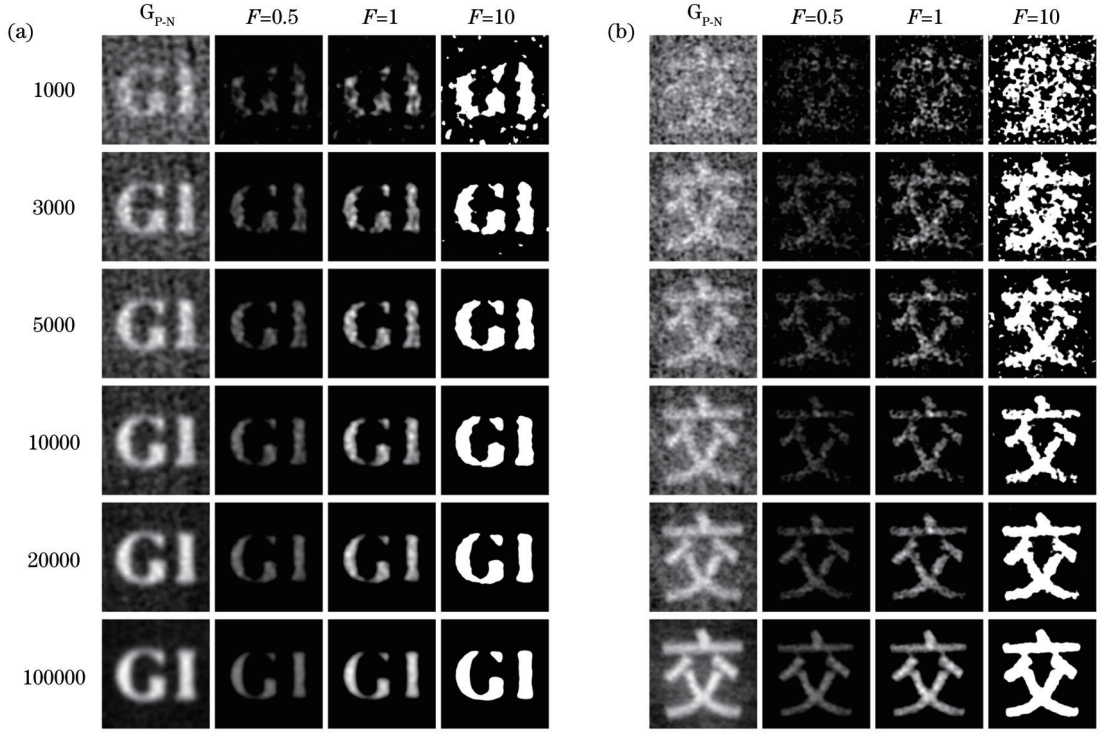

图 9　正负关联成像的优化。(a)字母“GI”;(b)汉字“交”

Fig. 9　Optimization of positive and negative correlation imaging. (a) English letters "GI"; (b) Chinese character "jiao"

4　结　　论

本文在传统鬼成像原理的基础上,设计研制了时序可控的赝热光鬼成像系统,该系统能够对鬼成像的散斑尺寸和采集次数实现精细控制并集成不同的成像算法,可以提高不同物体的成像质量。实验结果表明,

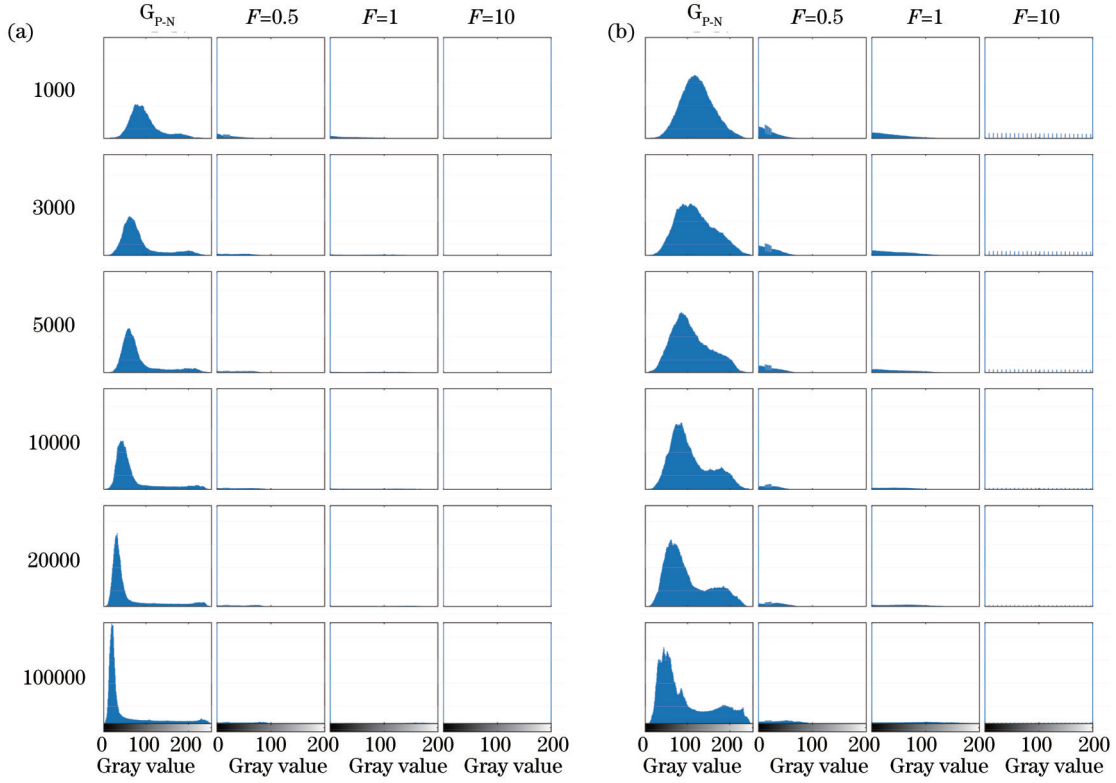

图 10 正负关联算法的优化成像直方图对比。(a)“GI”的直方图对比;(b)“交”的直方图对比

Fig. 10 Comparison of optimized histograms of positive and negative correlation algorithm. (a) Comparison of histograms for "GI"; (b) comparison of histograms for "jiao"

该系统的时序控制性能和算法的优化改善了传统赝热光鬼成像的成像质量。此外,在正负关联算法的基础上,通过对重构图像实现了二次优化,取得了显著的降噪效果。该系统性能和算法优化的成功实现,为研究更广泛用途和更为复杂环境下的鬼成像系统提供了借鉴。

参 考 文 献

[1] Pittman T B, Shih Y H, Strekalov D V, et al. Optical imaging by means of two-photon quantum entanglement[J]. Physical Review A, 1995, 52(5): R3429-R3432.

[2] Strekalov D V, Sergienko A V, Klyshko D N, et al. Observation of two-photon “ghost” interference and diffraction [J]. Physical Review Letters, 1995, 74(18): 3600-3603.

[3] Bennink R S, Bentley S J, Boyd R W. Two-photon coincidence imaging with a classical source[J]. Physical Review Letters, 2002, 89(11): 113601.

[4] Gatti A, Brambilla E, Bache M, et al. Ghost imaging with thermal light: comparing entanglement and classical correlation [J]. Physical Review Letters, 2004, 93(9): 093602.

[5] Scarcelli G, Berardi V, Shih Y. Can two-photon correlation of chaotic light be considered as correlation of intensity fluctuations? [J]. Physical Review Letters, 2006, 96(6): 063602.

[6] Basano L, Ottonello P. Experiment in lensless ghost imaging with thermal light[J]. Applied Physics Letters, 2006, 89(9): 091109.

[7] Shapiro J H. Computational ghost imaging[J]. Physical Review A, 2008, 78(6): 061802.

[8] Bromberg Y, Katz O, Silberberg Y. Ghost imaging with a single detector[J]. Physical Review A, 2009, 79(5): 053840.

[9] 高荣科, 严露沙, 徐陈祥, 等. 影响计算鬼成像质量的两种关键技术[J]. 激光与光电子学进展, 2021, 58(18): 1811011.
Gao R K, Yan L S, Xu C X, et al. Two key technologies influencing on computational ghost imaging quality[J]. Laser & Optoelectronics Progress, 2021, 58(18): 1811011.

[10] Yu H, Lu R H, Han S S, et al. Fourier-transform ghost imaging with hard X rays[J]. Physical Review Letters, 2016, 117(11): 113901.

[11] Pelliccia D, Rack A, Scheel M, et al. Experimental X-ray ghost imaging[J]. Physical Review Letters, 2016, 117(11): 113902.

[12] Zhang A X, He Y H, Wu L A, et al. Table-top X-ray ghost imaging with ultra-low radiation[J]. Optica, 2017, 5(4): 374-377.

[13] Watts C M, Shrekenhamer D, Montoya J, et al. Terahertz compressive imaging with metamaterial spatial light modulators [J]. Nature Photonics, 2014, 8(8): 605-609.

[14] Diebold A V, Imani M F, Sleasman T, et al. Phaseless coherent and incoherent microwave ghost imaging with dynamic metasurface apertures[J]. Optica, 2018, 5(12): 1529-1541.

[15] Li S, Cropp F, Kabra K, et al. Electron ghost imaging[J]. Physical Review Letters, 2018, 121(11): 114801.

[16] Khakimov R I, Henson B M, Shin D K, et al. Ghost imaging with atoms[J]. Nature, 2016, 540(7631): 100-103.

[17] Kingston A M, Myers G R, Pelliccia D, et al. Neutron ghost imaging[J]. Physical Review A, 2020, 101(5): 053844.

[18] He Y H, Huang Y Y, Zeng Z R, et al. Single-pixel imaging with neutrons[J]. Science Bulletin, 2021, 66(2): 133-138.

[19] Sun B, Edgar M P, Bowman R, et al. 3D computational imaging with single-pixel detectors[J]. Science, 2013, 340 (6134): 844-847.

[20] Bai B, He Y C, Liu J B, et al. Imaging around corners with single-pixel detector by computational ghost imaging[J]. Optik, 2017, 147: 136-142.

[21] Magaña-Loaiza O S, Howland G A, Malik M, et al.

Compressive object tracking using entangled photons[J]. Applied Physics Letters, 2013, 102(23): 231104.
[22] Jiang W J, Li X Y, Peng X L, et al. Imaging high-speed moving targets with a single-pixel detector[J]. Optics Express, 2020, 28(6): 7889-7897.
[23] Sun S, Hu H K, Xu Y K, et al. Simultaneously tracking and imaging a moving object under photon crisis[J]. Physical Review Applied, 2022, 17(2): 024050.
[24] Le M N, Wang G, Zheng H B, et al. Underwater computational ghost imaging[J]. Optics Express, 2017, 25(19): 22859-22868.
[25] 杨莫愁, 吴仪, 冯国英. 水下鬼成像的研究进展[J]. 光学学报, 2022, 42(17): 1701003.
Yang M C, Wu Y, Feng G Y. Research progress on underwater ghost imaging[J]. Acta Optica Sinica, 2022, 42(17): 1701003.
[26] Zhang P L, Gong W L, Shen X, et al. Correlated imaging through atmospheric turbulence[J]. Physical Review A, 2010, 82(3): 033817.
[27] Meyers R E, Deacon K S, Shih Y. Turbulence-free ghost imaging[J]. Applied Physics Letters, 2011, 98(11): 111115.
[28] Zhao C Q, Gong W L, Chen M L, et al. Ghost imaging lidar via sparsity constraints[J]. Applied Physics Letters, 2012, 101(14): 141123.
[29] Sun Z, Tuitje F, Spielmann C. Toward high contrast and high-resolution microscopic ghost imaging[J]. Optics Express, 2019, 27(23): 33652-33661.
[30] 冯悦姝, 周成, 刘轩, 等. 基于Hadamard优化矩阵的多分辨显微关联成像研究[J]. 光学学报, 2021, 41(21): 2111001.
Feng Y S, Zhou C, Liu X, et al. Study of multi-resolution microscopic correlation imaging based on optimized Hadamard matrix[J]. Acta Optica Sinica, 2021, 41(21): 2111001.
[31] Gong W L, Han S S. Correlated imaging in scattering media[J]. Optics Letters, 2011, 36(3): 394-396.
[32] Xu Y K, Liu W T, Zhang E F, et al. Is ghost imaging intrinsically more powerful against scattering? [J]. Optics Express, 2015, 23(26): 32993-33000.
[33] Ferri F, Magatti D, Lugiato L A, et al. Differential ghost imaging[J]. Physical Review Letters, 2010, 104(25): 253603.
[34] Sun B Q, Welsh S S, Edgar M P, et al. Normalized ghost imaging[J]. Optics Express, 2012, 20(15): 16892-16901.
[35] Sun M J, Li M F, Wu L A. Nonlocal imaging of a reflective object using positive and negative correlations[J]. Applied Optics, 2015, 54(25): 7494-7499.
[36] 刘雪峰, 姚旭日, 李明飞, 等. 强度涨落在热光鬼成像中的作用[J]. 物理学报, 2013, 62(18): 184205.
Liu X F, Yao X R, Li M F, et al. The role of intensity fluctuations in thermal ghost imaging[J]. Acta Physica Sinica, 2013, 62(18): 184205.
[37] Wang Z, Bovik A C, Sheikh H R, et al. Image quality assessment: from error visibility to structural similarity[J]. IEEE Transactions on Image Processing, 2004, 13(4): 600-612.
[38] Gao C, Wang X Q, Wang Z F, et al. Optimization of computational ghost imaging[J]. Physical Review A, 2017, 96(2): 023838.
[39] Chan K W C, O'Sullivan M N, Boyd R W. Optimization of thermal ghost imaging: high-order correlations vs. background subtraction[J]. Optics Express, 2010, 18(6): 5562-5573.
[40] Ferri F, Magatti D, Gatti A, et al. High-resolution ghost image and ghost diffraction experiments with thermal light[J]. Physical Review Letters, 2005, 94(18): 183602.
[41] Gong W L, Zhang P L, Shen X, et al. Ghost "pinhole" imaging in Fraunhofer region[J]. Applied Physics Letters, 2009, 95(7): 071110.
[42] Cao D Z, Xiong J, Zhang S H, et al. Enhancing visibility and resolution in Nth-order intensity correlation of thermal light[J]. Applied Physics Letters, 2008, 92(20): 201102.

Sequence-Controlled Pseudothermal Optical Ghost Imaging System

Zong Yanfeng, Zheng Huaibin*, Wu Xinwei, Li Jingwei, Qiu Long, Han Yuyuan

Electronic Materials Research Laboratory, Key Laboratory of the Ministry of Education & International Center for Dielectric Research, School of Electronic Science and Engineering, Xi'an Jiaotong University, Xi'an 710049, *Shaanxi, China*

Abstract

Objective Since its inception, ghost imaging technology has drawn wide interest and has been reported in many application scenarios due to its advantages, including strong anti-scattering capacity, lens-free imaging, and off-object imaging. In practice, however, ghost imaging technology still struggles with a number of fundamental issues, such as reliable signal recognition and quick imaging in challenging situations. These requirements call for more sophisticated algorithms, as well as hardware design and control. In this study, we design and develop a sequence-controlled ghost imaging system on the basis of the pseudothermal light ghost imaging technology scheme, which can achieve high-quality imaging under various conditions by precisely controlling the main components of the system. Apart from the fundamental correlation imaging algorithm, this system presents three more imaging algorithms, namely, differential ghost imaging, normalized ghost imaging, and positive-negative correlation imaging. A secondary optimization scheme for the images reconstructed by the positive-negative correlation algorithm is proposed to further improve the imaging quality. For the development of ghost imaging systems for a larger range of applications and more complicated situations, we hope that our system can serve as a model.

Methods In this paper, the sequence control capability of the ghost imaging system and the algorithm's optimization impact on the imaging quality are demonstrated through comparison tests. Figure 1 (a) is the schematic diagram of the

pseudothermal light ghost imaging system. Figure 1 (b) is the GUI interface of the system, through which the operations of the system can be directly controlled, such as the position of the displacement platform, the speed of the ground glass, the sampling times, and the imaging algorithm. The synchronous control of the system and the control of the electric displacement platform are realized by the control unit while the signal acquisition is completed. In addition, the differential ghost imaging, normalized ghost imaging, as well as positive-negative correlation algorithm and its optimization algorithm, are integrated to further improve the performance of the ghost imaging system.

The system′s sequence control performance is empirically demonstrated by research on the precise control of the speckle size and the sufficient sampling times for higher-quality imaging under different conditions. Comparison experiments of traditional ghost imaging, differential ghost imaging, normalized ghost imaging, and positive-negative correlation imaging and its optimized algorithm are conducted for various objects to verify the optimization effect of the system′s algorithm on the imaging quality.

Results and Discussions The system improves the imaging quality via both precise hardware control and an optimized algorithm (Fig. 1). The research shows that the speckle size of the object surface directly affects the imaging quality, and this system can accurately adjust the speckle size by controlling the relevant components to image objects of different sizes with the optimal resolution. In the experiment, two objects of different sizes are selected; the speckle size is adjusted, and the imaging with different speckle sizes is compared. The effect of the speckle size on the imaging quality and the optimal speckle sizes corresponding to different objects can be found through observations of the quality curves (Figs. 2 and 3). In addition, since traditional pseudothermal light ghost imaging requires sufficient sampling to achieve higher-quality imaging, the system generates a large amount of effective data by controlling the position of the rotating glass to satisfy this requirement (Figs. 4 and 5). Meanwhile, different imaging algorithms are combined in the system to optimize the imaging effect to a certain extent for different objects. In the comparison experiments of traditional ghost imaging with differential ghost imaging and normalized ghost imaging, the optimization effects of differential ghost imaging and normalized ghost imaging on imaging quality are confirmed. Both have a similar noise reduction effect under a large sampling times, and the optimization effect on different transmission-type objects also differs (Figs. 6 and 7). Meanwhile, noise reduction is performed again on the reconstructed images of the positive-negative correlation algorithm. It is found that the imaging noise is significantly reduced, and the value of the modulation factor is changed to avoid serious loss of some information on the object during noise reduction for optimal imaging results (Figs. 9 and 10).

Conclusions Based on the principle of traditional pseudothermal light ghost imaging, we designed and developed a sequence-controlled pseudothermal light ghost imaging system, which could achieve precise control of the speckle size and quantity of sampling for ghost imaging, while combining different imaging algorithms and proposing further optimization schemes to finally improve the imaging quality for different objects.

Key words imaging systems; ghost imaging system; synchronous control; imaging algorithm; imaging quality